DESIGN OF CAPACITIVE BULK-MICROMACHINED ACCELEROMETERS USING THE TOPOLOGY OPTIMIZATION METHOD

André da Costa Teves, andreteves@gmail.com
Emílio Carlos Nelli Silva, ecnsilva@usp.br
School of Engineering, University of São Paulo, 05508-010, Sao Paulo/SP - Brazil

Abstract. *A capacitive MEMS (Micro-Electromechanical Systems) accelerometer based on bulk-micromachining technology is generally fabricated using three wafers (glass, silicon, glass), bonded together one on top of the other, forming two sets of parallel plate capacitors: the middle layer is obtained by silicon etching processes and consists of an inertial mass supported by one or more beams (movable electrode); the top and bottom wafers form the fixed electrodes. The flexibility of the beams allows the mass to move proportionally to the external acceleration; the displacement is estimated by the change in capacitance of the two plates (differential measure). The design of such sensors is a complex task involving the maximization of the sensitivity, resolution, stability, bandwidth and the minimization of the power consumption, noise and cross-axis sensitivity. The main design parameters usually considered are: thickness of the gap, applied voltage, geometric dimensions of the inertial mass and beams, spatial configuration of the beams, thickness of the wafers, among others. In this paper, we apply the Topology Optimization Method (TOM) to the design of MEMS accelerometers using the SIMP (Solid Isotropic Material with Penalization) material model, in order to find the optimal topology for the middle layer of the sensor. The objective function is to maximize the sensitivity (V/g) and the bandwidth; a maximum volume restriction must also be satisfied. An algorithm implemented in Matlab uses the method of moving asymptotes (MMA) as optimizer and communicates with the software COMSOL to solve the finite element problem, which is based on the Reissner-Mindlin plate element, considering shear deformation, and the MITC (Mixed Interpolation of Tensorial Components) formulation. Finally, we present several topologies obtained for the sensor by varying the initial conditions.*

Keywords: *MEMS, accelerometers, topology optimization, Mindlin plate element*

1. INTRODUCTION

Micromachined accelerometers are one of the most important types of silicon-based sensors and one of the top sellers MEMS (Micro-Electromechanical Systems) devices, with annual worldwide sales topping 100 million units (Kaajakari, 2009). Starting in the 1990's up to few years ago, the large volume demand for microaccelerometers was due to their automotive applications, where they are used as crash sensors for air bag deployment, in Electronic Stability Control(ESC) and active suspension systems (Vigna, 2009).

In recent years, as the price of low-performance devices have dropped significantly, they have emerged as critical input devices for several consumer applications such as the latest generation of video games and cellphones for enhanced user interface, digital cameras for image stabilization, laptops for free-fall detection and many others. Whereas high-performance MEMS accelerometers are increasingly being used for inertial navigation, unmanned vehicles, seismographs and space instrumentation. With the continuing drop in prices, the number of applications for microaccelerometers should grow in coming years.

All types of acceleration sensors translate the external signal to the corresponding displacement of its proof mass that can be measured by various detection schemes, some of the most relevant are capacitive, piezoelectric, piezoresistive, resonant and optical. For a detailed review of the topic the reader is referred to Yazdi *et al.* (1998). This study focuses on the design of an electrostatic accelerometer. The main advantages of such transduction mechanism is that it presents high sensitivity, good dc response and noise performance, low temperature sensitivity and low-power consumption. However there are disadvantages that electromagnetic interference can be a great problem if the device is not properly packaged/shielded (MacDonald, 1990) and they are subjected to snap-down/pull-in (Kaajakari, 2009).

The two most commonly adopted designs for capacitive accelerometers are those with sensitivity to accelerations parallel (Mukherjee *et al.*, 1999; Coultate *et al.*, 2008) and perpendicular (Alvarez *et al.*, 2009; Takao *et al.*, 2001) to the silicon surface, they are usually implemented by surface and bulk-micromachining technology (Madou, 2002), respectively. The former generally uses a comb-like structure as sensing electrode, the thickness of the deposited layer and hence the proof mass is small, causing limitations on the performance of the accelerometers. On the other hand, in bulk micromachined devices, due to the presence of a large proof mass, higher resolution and greater sensitivity is achievable. Yazdi and Najafi (2000) proposed a combined aproach to further improve the sensor performance. In this paper, bulk-micromachined devices are considered.

In general, bulk-micromachined accelerometers are fabricated using three thick wafers, bonded together one on top of the other, forming two sets of parallel plate capacitors. The middle layer is obtained by silicon etching processes and

consists of a large proof mass suspended by one or more beams (movable electrode). It is separated by a narrow air gap from the top and bottom wafers, that form the two differential sense capacitors. Fig. 1 illustrates the cross-section of a typical design.

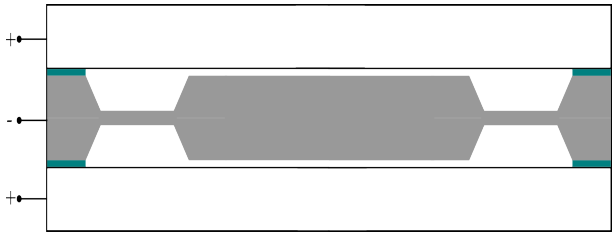

Figure 1. Typical bulk-micromachined accelerometer design.

The main feature that distinguishes a bulk-type design from others is the configuration of the suspension beams used. The seismic mass can be supported by one or more cantilevers (Rudolf *et al.*, 1990), by a torsion beam (Selvakumar *et al.*, 1996) or by folded-beams (Takao *et al.*, 2001). Currently, full-bridge and highly symmetrical designs using four or more beams (Yazdi and Najafi, 2000) are the most popular since they lead to very low cross-axis sensitivity. Some typical topologies are presented in Fig. 2.

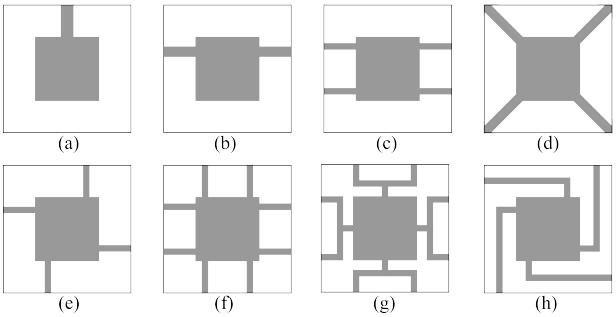

Figure 2. Typical suspension beams configuration in bulk-micromachined accelerometers: (a) single cantilever beam, (b) torsion beam, (c) full-bridge structure with four cantilevers, (d),(e),(f) symmetrical configurations with cantilevers, (g),(h) symmetrical configurations with folded beams.

The operation of MEMS sensors depend on many performance requirements, which are most often conflicting. In the case of accelerometers, in order to achieve high sensitivity it is necessary to reduce the air gap between the sense electrodes and increase the active area. However, reducing the air gap reduces the dynamic range of the sensor and lowers the pull-in voltage. On top of that, given its complex fabrication processes, each prototype iteration is very expensive. For these reasons optimization techniques are regularly used in the design stage of MEMS sensors, aiming to reduce development time and costs and simultaneously helping the designer to explore design trade-offs efficiently.

Most of the research in optimization of capacitive micro-accelerometers so far has been primarily focused on parametric analysis. Alvarez *et al.* (2009) aimed to maximize the bandwidth of a bulk-micromachined accelerometer, Liu *et al.* (2009) performed a robust optimization considering both bandwidth and sensitivity of a similar device and Desrochers *et al.* (2010) first optimized the shape of the hinges used in his bulk-design and then performed a multi-objective size optimization aiming the maximization of sensitivity and the minimization of the the ratio between the first and the second natural frequencies to reduce off-axis sensitivity. Mukherjee *et al.* (1999) and Coultate *et al.* (2008) presented analytical models for a surface-micromachined accelerometer similar to Analog Devices' ADXL family. The first considered the minimization of the footprint area and noise and maximization of the sensitivity, the latter presented a robust design considering maximization of the full-scale range (FSR) and minimization of the threshold acceleration.

An alternative approach widely used for optimal design is the Topology Optimization Method (TOM), which is a powerful structural optimization technique that reduces significantly the need for experienced designers and good physical intuition by providing a systematic approach for the design of structures. Combined with the finite element method, it solves the problem of finding the optimal distribution of material that maximizes a given objective function in a design domain subjected to applied loads and boundary conditions. Since its introduction by Bendsoe and Kikuchi (1988) the method has gained much popularity and is currently applied to a variety of structural optimization problems such as stiffness maximization (Suzuki and Kikuchi, 1991), eigenfrequency problems (Ma *et al.*, 1995; Pedersen, 2000), compliant mechanism design (Sigmund, 2001), piezoelectric actuator design (Silva *et al.*, 2000), among others.

However, few authors have published papers on TO of capacitive sensors. Krishnan and Ananthasuresh (2008) and Pedersen and Seshia (2004) proposed optimal designs for the springs of surface-micromachined accelerometers using

topology and size optimization methods with slightly distinct approaches. While Raulli and Maute (2005) and Liu *et al.* (2007) addressed the complex full electromechanically coupled problem using, respectively, staggered and monolithic analysis. However, they proposed optimal topologies for two and three-dimensional force inverter mechanisms, not sensors.

To the best knowledge of the authors, nothing has been published on TO of capacitive bulk-micromachined accelerometers. Therefore, in this research we propose a generic topology optimization formulation for the design of such devices. In particular, the optimal configuration for the suspension beams is pursued by taking into account sensitivity and bandwidth, two of the most important parameters when evaluating the performance of accelerometers. The goal is to optimize the topology of an accelerometer under development for applications in embedded systems such as aircraft, rockets, and satellites. This device (similar to Fig. 2h) is currently being developed within the project AcelerAD, of which the authors of this paper are members.

This paper is organized as follows. In Section 2, the FEM-based computational model is presented and the topology optimization problem formulation is discussed in detail. The numerical implementation is addressed in Section 3 and the results are presented in Section 4. Finally, Section 5 provides the concluding remarks and points to future developments.

2. TOPOLOGY OPTIMIZATION PROBLEM FORMULATION

2.1 Finite Element Formulation

At each iteration of the topology optimization procedure, a structural analysis has to be carried out, which is done using the Finite Element Method (FEM) (Bathe, 1996).

The structural problem considered here is solved using the software COMSOL, both stationary and eigenfrequency analysis are performed to account for the calculation of the output displacement and resonance frequencies. The middle layer of the accelerometer is modeled using a linear isoparametric 4-node Mindlin-Reissner-based plate with 6 degrees of freedom per node. The dependent variables are the displacements u, v, and w and the displacements of the plate normals ax, ay, and az in the global x, y, and z directions. This element overcomes the effects of shear locking by assuming a Mixed Interpolation of Tensorial Components (MITC) formulation (Chapelle and Bathe, 2003), which allows the use of thick layers. In Long *et al.* (2009) it is shown that this type of element is robust and reliable for use in structural topology optimization.

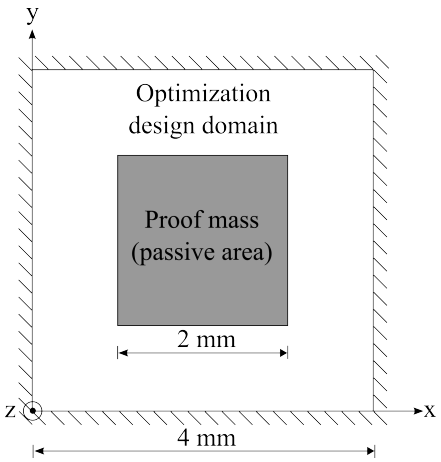

Figure 3. Finite element problem model.

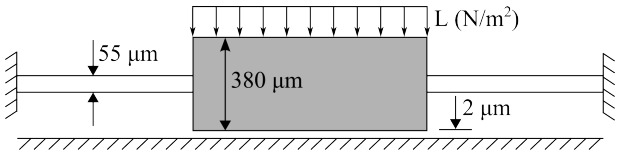

Figure 4. Cross section view of the middle layer of the accelerometer.

The model for the finite element problem is illustrated in Fig. 3 and its cross section in Fig. 4. The dimensions of the domain are chosen in this way to accurately represent the accelerometer that is currently being developed under the project AcelerAD.

The squared plate is clamped at all four edges and the dark region represents the proof mass, which is considered as a passive area, i.e, with full density during the entire optimization. The rest of the domain (white color) is where the optimization process will actually take place. A fixed distributed load L, representing the electrostatic force acting on the proof mass, is applied to the dark region - this is a purely mechanical load. As stated in Liu *et al.* (2007), if there is a predefined air gap (which is the case here), direction, magnitude and actuation area of electrostatic forces are fixed and thus topology optimization considering purely mechanical loads can be used to design capacitive devices.

For the stationary problem, the equilibrium equations to be solved can be written in the matrix form as:

$$\mathbf{KU} = \mathbf{F} \tag{1}$$

where $\mathbf{K}$ is the stiffness matrix, $\mathbf{U}$ is the nodal solution vector, and $\mathbf{F}$ is the load vector, they are all defined in Bathe

(1996). Whereas for the eigenfrequency analysis, considering only free vibrations, the equilibrium equations to be solved is given by:

$$\mathbf{M}\ddot{\mathbf{U}} + \mathbf{K}\mathbf{U} = \mathbf{0} \tag{2}$$

where $\mathbf{M}$ is the mass matrix (Bathe, 1996). The material used in the entire domain is silicon with the following properties: density $\rho = 2330kg/m^3$, Young's modulus $E = 170GPa$ and poisson ratio $\upsilon = 0.27$.

2.2 Material model

As stated earlier, TO seeks the optimal distribution of material inside a given design domain. A discrete characteristic function $\chi(\Omega)$ containing information about the material densities at each element can be considered as follows:

$$\chi(\Omega) = \begin{cases} 1 & \text{if material is present} \\ 0 & \text{if void} \end{cases} \tag{3}$$

However $\chi(\Omega)$ is highly discontinuous and will lead to numerical instabilities caused by multiple local minima (Sigmund and Petersson, 1998). Therefore, the Solid Isotropic Material Distribution (SIMP)(Bendsoe and Sigmund, 2003) approach is used to relax the problem by allowing the material to assume intermediate densities from zero to unity. In this case, at each point of the domain, the material property D (for instance, the elasticity tensor) is given by:

$$D = \rho^p D_0 \tag{4}$$

where D_0 is the property of the basic material that will be distributed in the domain, ρ is a pseudo-density that can assume values between 0 and 1 describing the amount of material at each point in the domain and p is a penalization factor to favor the ocurrence of black and white (0/1) solutions for manufacturing reasons. As we will be working with stationary and eigenfrequency analysis, both the stiffness matrix $\mathbf{K}$ and the mass matrix $\mathbf{M}$ are penalized using different penalization factors p_e and p_m, respectively. In order to avoid local modes (Pedersen, 2000), the following relationship must hold: $p_e > p_m$.

Although the SIMP method overcomes a major numerical problem, it is prone to the so-called checkerboard patterns, mesh dependency. These issues are addressed by the use of filtering techniques (Sigmund, 2007). In this work the filter proposed by Guest *et al.* (2004) is implemented.

2.3 Formulation of design problem

As mentioned earlier, both sensitivity and bandwidth are considered in the optimization problem. In capacitive accelerometers the sensitivity can be defined as the relative change of capacitance per unit of acceleration and its value is directly connected to the vertical deflection of the movable plate. Whereas the bandwidth is limited to $1/5$ of the first resonance frequency (Harris and Crede, 1976). In view of that, the vertical deflection, or the compliance (the inverse of stiffness), and the first resonance frequency should be maximized to improve the device performance with respect to sensitivity and bandwidth, respectively.

The mean compliance, also known as strain energy, is given by:

$$C = \mathbf{U}^T\mathbf{K}\mathbf{U} \tag{5}$$

where the superscript T stands for the transpose vector. In order to perform the optimization we need to calculate the gradients of the objective functions. The sensitivity $\dfrac{\partial C}{\partial \rho}$ is given by:

$$\frac{\partial C}{\partial \rho_e} = -\mathbf{U_e}^T \frac{\partial \mathbf{K_e}}{\partial \rho_e}\mathbf{U_e} \tag{6}$$

where the index e is a reference to the degrees of freedom of a specific element.

Concerning the maximization of the first eigenfrequency, a mean eigenvalue Λ (Eq. 7), which is a combination of multiple eigenvalues, is suggested by Ma *et al.* (1995). This formulation improves the convergence of the solution by reducing the discontinuity in the objective function caused by the eigenfrequency switching order during the optimization problem.

$$\Lambda = \alpha \left(\sum_{i=1}^{m} \frac{w_i}{\lambda_i - \lambda_0} \right)^{-1} \text{ with } \alpha = \sum_{i=1}^{m} w_i \text{ and } \lambda_i = \omega_i^2 \tag{7}$$

where ω_i is the resonance frequency associated with a specific mode of vibration, $w_i (i = 1, 2, \ldots, m)$ are weighting coefficients and λ_0 is a given parameter. If all the weighting coefficients w_i are the same, the eigenvalue which is the

closest to λ_0 will experience the largest increase in the optimization process. In most of our analysis we used $w_i = 1$, $\lambda_0 = 0$ and $m = 6$.

The sensitivity $\dfrac{\partial \Lambda}{\partial \rho}$ is found as:

$$\frac{\partial \Lambda}{\partial \rho_e} = \frac{\Lambda^2}{\alpha} \sum_{i=1}^{m} \frac{w_i}{(\lambda_i - \lambda_0)^2} \frac{\partial \lambda_i}{\partial \rho_e} \tag{8}$$

with:

$$\frac{\partial \lambda_i}{\partial \rho_e} = \phi_{i,e}^T \left(\frac{\partial \mathbf{K_e}}{\partial \rho_e} - \lambda_i \frac{\partial \mathbf{M_e}}{\partial \rho_e} \right) \phi_{i,e} \tag{9}$$

where $\phi_{i,e}$ is the eigenvector associated with the eigenvalue λ_i and $\mathbf{M_e}$ is the element mass matrix.

2.4 The optimization problem

The problem studied here is not trivial, since it involves two conflicting requirements and the design domain is limited by the passive area. For this reason several formulations are tested, the two simplest ones being the minimization of the mean compliance C and the maximization of the mean eigenvalue Λ, as stated in Problems (I) and (II).

$$\begin{aligned} \underset{\rho}{\text{Minimize}} \quad & C \\ \text{subject to} \quad & \mathrm{V} = \sum_{i=1}^{n_e} \rho_e V_e \leq \mathrm{V}_{\max} \\ & 0 < \rho_{min} \leq \rho \leq 1 \end{aligned} \tag{I}$$

$$\begin{aligned} \underset{\rho}{\text{Maximize}} \quad & \Lambda \\ \text{subject to} \quad & \mathrm{V} \leq \mathrm{V}_{\max} \\ & 0 < \rho_{min} \leq \rho \leq 1 \end{aligned} \tag{II}$$

where n_e is the total number of elements in the design domain and V_e is volume of the individual elements. The first constraint is a limitation on the material volume allowed to be distributed. Combined with the SIMP power-law, it minimizes the raise of grey regions and favour the occurrence of narrow structures with thin bars and members that can be quickly under-etched during fabrication (Sigmund, 2001). The limit ρ_{min} for ρ is necessary to avoid numerical problems in the FE problem, it is chosen as $\rho_{min} = 1 \times 10^{-6}$ and for all practical reasons they can be considered holes in the final topology.

Next, the previous two problems are combined in a multi-objective function in Problem (III):

$$\begin{aligned} \underset{\rho}{\text{Maximize}} \quad & \mathcal{F} = ylnC + (1-y)ln\Lambda \\ \text{subject to} \quad & \mathrm{V} \leq \mathrm{V}_{\max} \\ & 0 < \rho_{min} \leq \rho \leq 1 \end{aligned} \tag{III}$$

where y is a weighting coefficient $(0 \leq y \leq 1)$, which allows us to control the contribution of the two conflicting objective functions. The natural logarithm is used in order to normalize the values of the functions, other normalization factors are also tested.

In the next two formulations (Problems IV and V), we moved one of the requirements to the constraints and kept the other as objective function.

$$\begin{aligned} \underset{\rho}{\text{Maximize}} \quad & C \\ \text{subject to} \quad & \Lambda \leq \overline{\Lambda} \\ & \mathrm{V} \leq \mathrm{V}_{\max} \\ & 0 < \rho_{min} \leq \rho \leq 1 \end{aligned} \tag{IV}$$

$$\begin{aligned} \underset{\rho}{\text{Maximize}} \quad & \Lambda \\ \text{subject to} \quad & C \geq \overline{C} \\ & \mathrm{V} \leq \mathrm{V}_{\max} \\ & 0 < \rho_{min} \leq \rho \leq 1 \end{aligned} \tag{V}$$

where $\overline{C}$ and $\overline{\Lambda}$ are the lower limits for the respective constraints. Finally, three other problems (VI, VII and VIII) are considered with the volume being used as objective function.

$$\begin{aligned} \underset{\rho}{\text{Maximize}} \quad & \mathrm{V}^* = \sum_{i=1}^{n_e} \rho_e^{p_v} V_e \\ \text{subject to} \quad & C \geq \overline{C} \\ & 0 < \rho_{min} \leq \rho \leq 1 \end{aligned} \tag{VI}$$

$$\begin{aligned} \underset{\rho}{\text{Maximize}} \quad & \mathrm{V}^* \\ \text{subject to} \quad & \Lambda \leq \overline{\Lambda} \\ & 0 < \rho_{min} \leq \rho \leq 1 \end{aligned} \tag{VII}$$

Similarly to what we have done before, the objective function is penalized with p_v. At last, Problems (VI) and (VII) are combined generating Problem(VIII).

$$\begin{array}{ll} \underset{\rho}{\text{Maximize}} & \mathrm{V}^* \\ \text{subject to} & C \geq \overline{C} \\ & \Lambda \leq \overline{\Lambda} \\ & 0 < \rho_{min} \leq \rho \leq 1 \end{array} \tag{VIII}$$

The advantages and drawbacks of each of these formulations are discussed in section 4, the resulting topologies are also presented.

3. NUMERICAL IMPLEMENTATION

A flow chart of the optimization algorithm is shown in Fig. 5. The code is implemented in Matlab using COMSOL as the finite element problem solver. The gradients of the objective function and constraints are linearized by developing them into Taylor series up to the linear term. They are used as input for the optimization problem, that is solved using the Method of Moving Asymptotes (MMA) (Svanberg, 1987). The optimizer generates a new set of design variables ρ after each iteration and the optimization continues until convergence is achieved for the objective function.

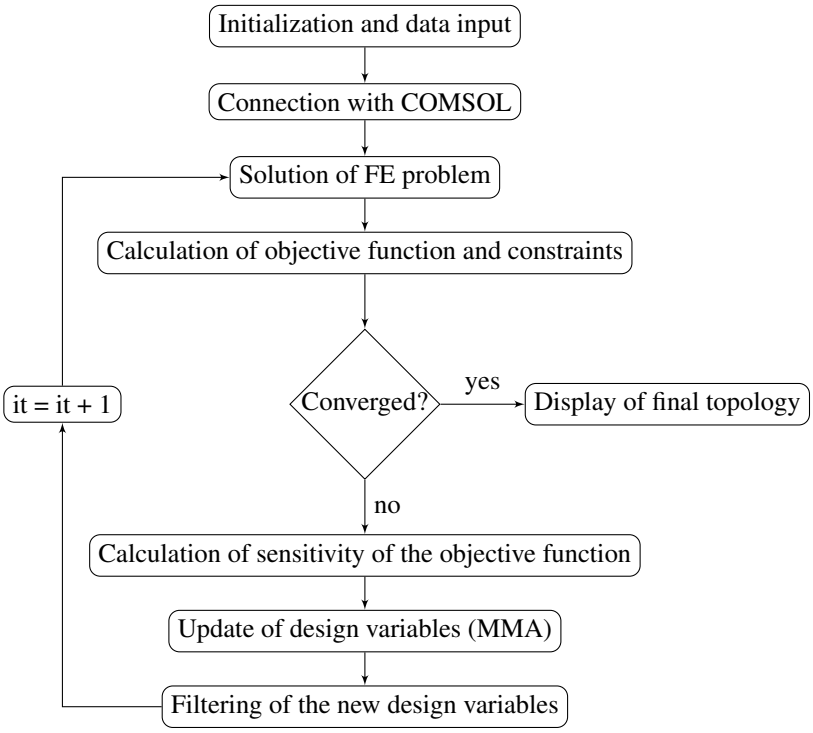

Figure 5. Flowchart of optimization procedure.

4. RESULTS

Unless otherwise noticed, the AcelerAD topology (see Fig. 6) is used as initial guess in all problems presented in this section. Besides that, the filter radius is set to $200\mu m$, the penalty factor p_e varied from 1 to 3 and p_m from 1 to 6 along the first 20 optimization cycles. The domain shown in Fig. 3 is discretized in 40x40 elements.

Problems (I) and (II) are solved with $V_{max} = 0.60$ and the post-processed topologies obtained are plotted in Fig. 7 and Fig. 8, respectively. The values of the first and the second resonance frequencies, the output displacement and the strain energy are listed in Tab. 1. Although the topologies are quite different, the bandwidth and the displacement are almost the same for the two problems.

The problem formulation (III), the multi-objective attempt, did not produce good results. Several studies were run using different sets of parameters such as filter radius, maximum volume allowed, penalization factors, different initial guesses and normalization factors for both components of the objective function. However no attempt has succeeded to generate a continuous topology so far. We believe that this has been caused by the large difference (> 1000x) in the gradients of the two components of the objective function. This way, we could not use the weighting coefficient y to explore the Pareto-optimal set.

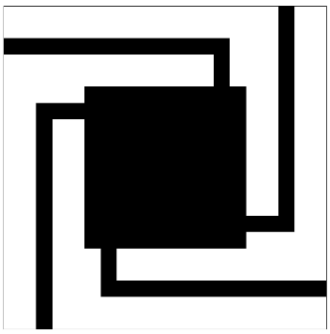

Figure 6. Initial guess (AcelerAD).

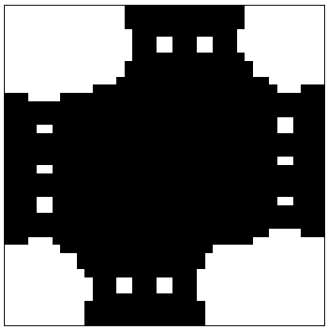

Figure 7. Resulting topology of optimization problem (I).

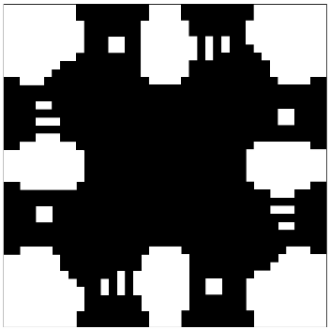

Figure 8. Resulting topology of optimization problem (II).

From now on, we set $m = 1$ in Eq. 7, i.e., only the first resonance frequency is considered in the optimization process. Thus, $\overline{f}$ is used instead of $\overline{\Lambda}$ to reference the frequency constraint limitation. In Problem (IV), the best result is obtained by using $V_{max} = 0.45$ with $\overline{f} = 15kHz$. The resulting structure is presented in Fig. 9 and the other results are listed in Tab. 1.

The difference between the lower boundary $\overline{f}$ and the first resonance frequency is explained by the presence of all the elements in the mesh during the optimization process. No matter how small their pseudo-density is, the 'empty' elements influence the system response, making it more stiff. At the end of optimization, the geometry is post-processed by defining a cut-off density $\overline{\rho}$, below which all elements are actually removed from the domain. This new topology, considering only those elements with pseudo-density $\rho_e > \overline{\rho}$, is simulated in COMSOL and the values of the first resonance frequencies, the displacement and the strain energy are obtained. This procedure is illustrated by observing Fig. 10, the raw topology, and Fig. 9, the result after post-processing.

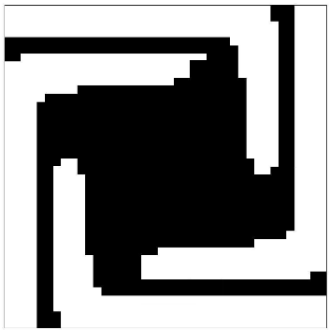

Figure 9. Resulting topology of optimization problem (IV) after post-processing.

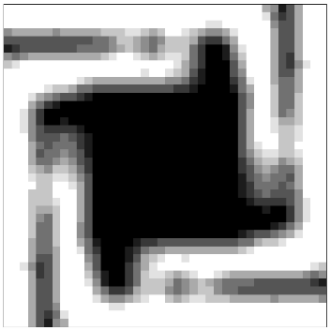

Figure 10. Raw result of optimization problem (IV).

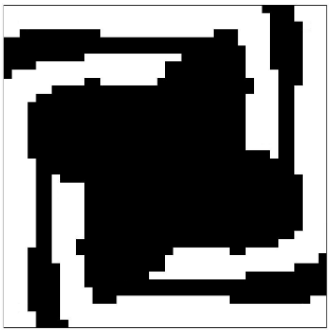

Figure 11. Resulting topology of optimization problem (V) using seed layer.

At first, Problem (V) did not produce good results, i.e., continuous topologies. Only when the initial guess is kept fixed as full density during all optimization cycles (seed layer), is that it can generate good topologies. Under this condition, the result obtained with $V_{max} = 0.60$ and $\overline{C} = 1 \times 10^{-12} Nm$ is shown in Fig. 11. An important remark about Problem (IV) and (V) is that, even if indirectly, they can be used to tune the structure to a desired output displacement or to a desired resonance frequency.

This statement also holds for the next three formulations considered. Besides that, in the next formulations the volume constraint is not needed anymore. It should be made clear that there is no practical reason (from the fabrication point of view) for the use of such constraint, other than its key importance to reduce gray scale in the previous formulations.

Jumping to Problem (VII), this is certainly the one that presented the best results as it is less sensitive to variation of the initial parameters, showing very good convergence. Figures 12-14 show the results for different values of $\overline{f}$ - the possibility to indirectly tune the structure to a specific resonance frequency is made clear with this example.

Problem (VI) is solved by using $\overline{C} = 1 \times 10^{-12} Nm$ and the resulting topology is presented in Fig. 15.

Finally, similarly to Problems (III) and (V), at first Problem (VIII) did not produce any good result either. Once again we had to use a seed layer to get a reasonable topology from this formulation. As it can be observed in Fig. 16, by using $\overline{C} = 1 \times 10^{-11} Nm$ and $\overline{f} = 9kHz$, the result is very close to the AcelerAD topology. From Tab. 1, it is also possible to say that both topologies have very similar performance requirements. This is an indication that the design initially suggested in the AcelerAD project is close to optimal.

A fact should be noted in problems involving the maximization of the volume (VI - VIII): the rise of islands and the

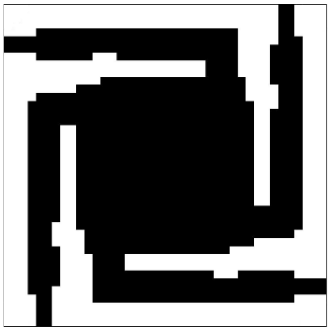

Figure 12. Problem (VII)-a: $\overline{f}$ set to $4kHz$.

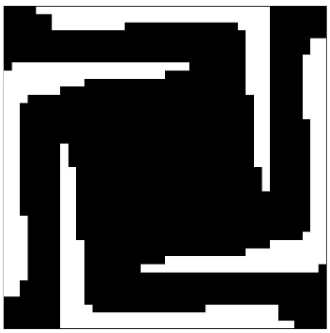

Figure 13. Problem (VII)-b: $\overline{f}$ set to $9kHz$.

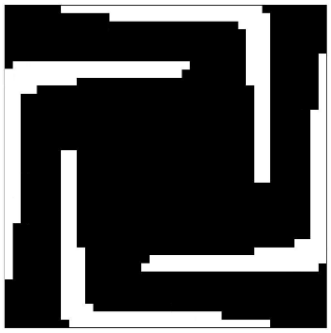

Figure 14. Problem (VII)-c: $\overline{f}$ set to $15kHz$.

addition of material in regions of the domain that are not under significant mechanical stress, as shown in the corners of Fig. 17, which is the raw topology of Fig. 16. These patterns should be removed during the post-processing phase as they are actually a shortcut used by the optimizer to maximize the volume without affecting much the system response.

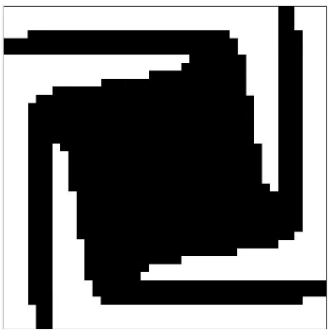

Figure 15. Resulting topology for optimization problem (VI).

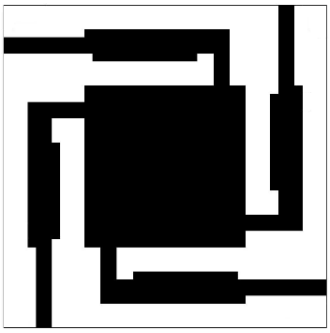

Figure 16. Resulting topology for optimization problem (VIII) using seed layer.

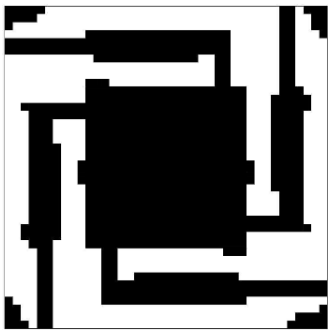

Figure 17. Raw result of optimization problem (VIII) using seed layer.

Table 1. Results Summary

Problem	1^{st} / 2^{nd} Res. freqs. (kHz)	Output disp. @ 1g (nm)	Strain energy @ 1g (Nm)
I	36.6 / 63.6	0.19	7.35×10^{-15}
II	37.1 / 70.7	0.18	7.45×10^{-15}
III	-	-	-
IV	3.4 / 7.0	20.78	7.8×10^{-13}
V	4.3 / 8.1	13.29	1.3×10^{-12}
VI	3.2 / 6.9	24.25	1.1×10^{-12}
VII-a	3.1 / 6.7	26.84	-
VII-b	4.8 / 10.1	10.8	-
VII-c	6.1 / 11.8	6.94	-
VIII	2.6 / 6.1	36.59	1.3×10^{-12}
AcelerAD	2.4 / 5.6	42.94	1.6×10^{-12}

5. CONCLUSIONS

Several formulations for the design of MEMS capacitive bulk-accelerometer using topology optimization are presented. It is demonstrated that some of them are not as successful as others in finding optimal topologies for the proposed problem, that is case of formulations (III), (V) and (VIII). The difficulty faced by those approaches might be explained by the conflicting behaviour of the two requirements involved: sensitivity and resonance frequencies.

The algorithm implemented here could not generate topologies with larger sensitivities than the initially proposed design (AcelerAD), however the bandwidth is increased in all the different methods used. It is worth noting that this

problem is not exhausted, new attempts will be made to better suit the two conflicting goals.

From the standpoint of manufacturing, the proposed topologies are not manufacturable using the inexpensive KOH etching, since they do not present straight angles, as in case of the AcelerAD design. However they can be fabricated using more complex processes. New topology optimization techniques that can take this requirement into account are currently being studied.

Finally, it is important to mention that the optimization performed is purely deterministic, i.e., the uncertainties involved in the operation and fabrication of the accelerometer are not taken into account. Considering their size and the relatively large manufacturing tolerances, a robust design is a key feature for high performance MEMS devices. This study is planned to be developed in future works.

6. ACKNOWLEDGMENTS

The first author acknowledges FINEP (Brazilian Agency for Funding of Studies and Projects) for providing scholarship support, under grant 01.09.0395.00 through the project AcelerAD. The second author thanks the financial support of CNPq (National Council for Research and development) under grant 303689/2009-9. The authors are grateful to Krister Svanberg from KTH Royal Institute of Technology for suppling the MMA-code and also to Prof. Akihiro Takezawa from Hiroshima University for providing a sample topology optimization code with COMSOL as the finite element solver.

7. REFERENCES

Alvarez, M.J., Gil-Negrete, N., Ilzarbe, L., Tanco, M., Viles, E. and Asensio, A., 2009. "A computer experiment application to the design and optimization of a capacitive accelerometer". *Applied Stochastic Models in Business and Industry*, Vol. 25, No. 2, pp. 151–162.

Bathe, K.J., 1996. *Finite Element Procedures*. Prentice Hall.

Bendsoe, M.P. and Sigmund, O., 2003. *Topology Optimization: Theory, Methods and Applications*. Springer Verlag.

Bendsoe, M.P. and Kikuchi, N., 1988. "Generating optimal topologies in structural design using a homogenization method". *Comput. Methods Appl. Mech. Eng.*, Vol. 71, pp. 197–224.

Chapelle, D. and Bathe, K.J., 2003. *The Finite Element Analysis of Shells: Fundamentals*. Springer.

Coultate, J.K., Fox, C.H., McWilliam, S. and Malvern, A.R., 2008. "Application of optimal and robust design methods to a mems accelerometer". *Sensors and Actuators A: Physical*, Vol. 142, No. 1, pp. 88 – 96.

Desrochers, S., Pasini, D. and Angeles, J., 2010. "Optimum design of a compliant uniaxial accelerometer". *Journal of Mechanical Design*, Vol. 132, No. 4.

Guest, J.K., Prévost, J.H. and Belytschko, T., 2004. "Achieving minimum length scale in topology optimization using nodal design variables and projection functions". *International Journal for Numerical Methods in Engineering*, Vol. 61, No. 2, pp. 238–254.

Harris, C.M. and Crede, C.E., 1976. *Shock and Vibration Handbook*. McGraw-Hill, New York.

Kaajakari, V., 2009. *Practical MEMS*. Small Gear Publishing, Las Vegas.

Krishnan, G. and Ananthasuresh, G.K., 2008. "Evaluation and design of displacement-amplifying compliant mechanisms for sensor applications". *Journal of Mechanical Design*, Vol. 130, No. 10, p. 102304.

Liu, G.J., Jiang, T. and Wang, A.L., 2009. "Robust optimization of an accelerometer considering fabrication errors". *Materials Science Forum*, Vol. 628.

Liu, M., Maute, K. and Frangopol, D.M., 2007. "Multi-objective design optimization of electrostatically actuated microbeam resonators with and without parameter uncertainty". *Reliability Engineering & System safety*, Vol. 92, No. 10, pp. 1333–1343.

Long, C.S., Loveday, P.W. and Groenwold, A.A., 2009. "Effects of finite element formulation on optimal plate and shell structural topologies". *Finite Elem. Anal. Des.*, Vol. 45, pp. 817–825.

Ma, Z.D., Kikuchi, N. and Cheng, H.C., 1995. "Topological design for vibrating structures". *Computer Methods in Applied Mechanics and Engineering*, Vol. 121, No. 1-4, pp. 259 – 280.

MacDonald, G., 1990. "A review of low cost accelerometers for vehicle dynamics". *Sensors and Actuators A: Physical*, Vol. 21, No. 1-3, pp. 303 – 307.

Madou, M.J., 2002. *Fundamentals of Microfabrication: the science of miniaturization*. CRC Press.

Mukherjee, T., Zhou, Y. and Fedder, G., 1999. "Automated optimal synthesis of microaccelerometers". In *Micro Electro Mechanical Systems, 1999. MEMS '99. Twelfth IEEE International Conference on*. pp. 326 –331.

Pedersen, C.B.W. and Seshia, A.A., 2004. "On the optimization of compliant force amplifier mechanisms for surface micromachined resonant accelerometers". *Journal of Micromechanics and Microengineering*, Vol. 14, No. 10, p. 1281.

Pedersen, N.L., 2000. "Maximization of eigenvalues using topology optimization". *Structural and Multidisciplinary Optimization*, Vol. 20, pp. 2–11.

Raulli, M. and Maute, K., 2005. "Topology optimization of electrostatically actuated microsystems". *STRUCTURAL*

AND MULTIDISCIPLINARY OPTIMIZATION, Vol. 30, No. 5, pp. 342–359.

Rudolf, F., Jornod, A., Bergqvist, J. and Leuthold, H., 1990. "Precision accelerometers with [mu]g resolution". *Sensors and Actuators A: Physical*, Vol. 21, No. 1-3, pp. 297 – 302.

Selvakumar, A., Ayazi, F. and Najafi, K., 1996. "A high sensitivity z-axis torsional silicon accelerometer". In *Electron Devices Meeting, 1996. IEDM '96., International*. pp. 765 –768.

Sigmund, O., 2001. "Design of multiphysics actuators using topology optimization - part i: One-material structures". *Computer Methods in Applied Mechanics and Engineering*, Vol. 190, No. 49-50, pp. 6577 – 6604.

Sigmund, O., 2007. "Morphology-based black and white filters for topology optimization". *Structural and Multidisciplinary Optimization*, Vol. 33, pp. 401–424.

Sigmund, O. and Petersson, J., 1998. "Numerical instabilities in topology optimization: A survey on procedures dealing with checkerboards, mesh-dependencies and local minima". *Structural Optimization*, Vol. 16, pp. 68–75.

Silva, E., Nishiwaki, S. and Kikuchi, N., 2000. "Topology optimization design of flextensional actuators". *IEEE Transactions on Ultrasonics, Ferroelectrics, and Frequency Contro*, Vol. 47, No. 3, pp. 657–671.

Suzuki, K. and Kikuchi, N., 1991. "A homogenization method for shape and topology optimization". *Computer Methods in Applied Mechanics and Engineering*, Vol. 93, No. 3, pp. 291 – 318.

Svanberg, K., 1987. "The method of moving asymptotes: a new method for structural optimization". *International Journal for Numerical Methods in Engineering*, Vol. 24, No. 2, pp. 359–373.

Takao, H., Fukumoto, H. and Ishida, M., 2001. "A cmos integrated three-axis accelerometer fabricated with commercial submicrometer cmos technology and bulk-micromachining". *Electron Devices, IEEE Transactions on*, Vol. 48, No. 9, pp. 1961 –1968.

Vigna, B., 2009. "Mems epiphany". In *Micro Electro Mechanical Systems, 2009. MEMS 2009. IEEE 22nd International Conference on*. pp. 1 –6.

Yazdi, N., Ayazi, F. and Najafi, K., 1998. "Micromachined inertial sensors". *Proceedings of the IEEE*, Vol. 86, No. 8, pp. 1640 –1659.

Yazdi, N. and Najafi, K., 2000. "An all-silicon single-wafer micro-g accelerometer with a combined surface and bulk micromachining process". *Journal ofMicroelectromechanical Systems*, Vol. 9, No. 4, pp. 544 –550.

8. Responsibility notice

The authors are the only responsible for the printed material included in this paper.